HHS Public Access

Author manuscript

Mol Cell. Author manuscript; available in PMC 2016 September 03.

Published in final edited form as:

Mol Cell. 2015 September 3; 59(5): 858–866. doi:10.1016/j.molcel.2015.07.023.

Tracking distinct RNA populations using efficient and reversible covalent chemistry

Erin E. Duffy[1,2], **Michael Rutenberg-Schoenberg**[1,2], **Catherine D. Stark**[1,2], **Robert R. Kitchen**[1], **Mark B. Gerstein**[1], and **Matthew D. Simon**[1,2,*]

[1]Department of Molecular Biophysics & Biochemistry, Yale University, New Haven, CT 06511, USA

[2]Chemical Biology Institute, Yale University, West Haven, CT 06516, USA

SUMMARY

We describe a chemical method to label and purify 4-thiouridine (s^4U)-containing RNA. We demonstrate that methanethiosulfonate (MTS) reagents form disulfide bonds with s^4U more efficiently than the commonly used HPDP-biotin, leading to higher yields and less biased enrichment. This increase in efficiency allowed us to use s^4U-labeling to study global microRNA (miRNA) turnover in proliferating cultured human cells without perturbing global miRNA levels or the miRNA processing machinery. This improved chemistry will enhance methods that depend on tracking different populations of RNA, such as 4-thiouridine-tagging to study tissue-specific transcription and dynamic transcriptome analysis (DTA) to study RNA turnover.

INTRODUCTION

RNA is continuously transcribed and degraded in a tightly regulated and transcript-specific manner. The dynamics of different RNA populations can be studied by targeted incorporation of non-canonical nucleosides. These nucleosides can provide a chemical handle for labeling and enriching RNA subpopulations. The labeling of RNA employs 5-bromouridine (5-BrU; Tani et al., 2012), 5-ethynyluridine (5-EU; Jao and Salic, 2008), and 4-thiouridine (TU or s^4U; Cleary et al., 2005; Miller et al., 2009), which provide different vehicles for antibody detection, cycloaddition reactions, and thiol-specific reactivity, respectively. 4-thiouridine holds the advantage that labeling is covalent, unlike the antibody

*Correspondence should be addressed to M.D.S. (matthew.simon@yale.edu).

Accession Codes

Raw and processed RNA-Seq data sets have been submitted NCBI Gene Expression Omnibus (http://www.ncbi.nlm.nih.gov/geo/) under the accession code GSE60988.

COMPETING FINANCIAL INTERESTS

The authors declare no competing financial interests.

Author contributions: E.E.D., M.R.S. and M.D.S. designed the study; E.E.D. and C.D.S. performed all experiments; M.R.S., processed and analyzed RNA-Seq data with assistance from R.R.K., M.B.G., E.E.D. and M.D.S.; E.E.D. and M.D.S. wrote the manuscript with input from M.R.S. and C.D.S.

detection of 5-BrU, and also that the disulfide bond is reversible, unlike the click chemistry used to label 5-EU (reviewed in(Tani and Akimitsu, 2012).

Methods to enrich s^4U-incorporated RNA (s^4U-RNA) initially relied on organomercurial affinity matrices (Melvin et al., 1978), but the use of s^4U in metabolic labeling expanded after HPDP-biotin, a 2-pyridylthio-activated disulfide of biotin, was developed as a practical means to biotinylate s^4U-RNA using reversible disulfide chemistry, followed by enrichment using a streptavidin matrix (Cleary et al., 2005; Dölken et al., 2008). The s^4U-RNAs can be eluted by reduction of the disulfide linkage and subsequently analyzed by microarray, qPCR, or deep sequencing. This modified protocol sparked a surge in techniques that use s^4U metabolic labeling. For example, half-lives of specific RNAs can be measured using s^4U metabolic labeling by quantifying the ratio of pre-existing (flow through) to newly transcribed (elution) RNA (Dölken et al., 2008). This approach has been extended to genome-wide analysis using high-throughput sequencing (s^4U-Seq; Rabani et al., 2011). Combining s^4U metabolic labeling with dynamic kinetic modeling has led to the development of dynamic transcriptome analysis (DTA; Miller et al., 2011), and comparative dynamic transcriptome analysis (cDTA) when using *S. pombe* standards for normalization, which allows the determination of absolute rates of mRNA synthesis and decay (Sun et al., 2012). Reversible transcriptional inhibition has been combined with s^4U metabolic labeling to measure transcriptional elongation rates (Fuchs et al., 2014). Recently, s^4U metabolic labeling has been used with approach to equilibrium kinetics to determine absolute RNA degradation and synthesis rates based on multiple time points after s^4U labeling (RATE-seq; Neymotin et al., 2014). In addition to these methods for analyzing RNA turnover, the enrichment of s^4U-RNA can also be used to determine cell-type specific transcription (4-thiouridine tagging), which is particularly helpful for analyzing the transcriptomes of cell types that are difficult to isolate by dissection or dissociation methods (Miller et al., 2009).

As the efficient chemical modification of s^4U is central to all of these techniques, we tested the reactivity of s^4U with HPDP-biotin. Here we report that the reaction and corresponding enrichment of s^4U-RNA with HPDP are inefficient. Therefore, we developed and validated chemistry using activated disulfides to label and enrich s^4U-RNA. This chemistry increases labeling yields and decreases enrichment bias. Due to the increased efficiency of this chemistry, we were able to extend s^4U-metabolic labeling to the study of microRNAs (miRNAs), providing insight into miRNA turnover in proliferating cells without inhibition of miRNA processing pathways. Our studies expand the utility of s^4U in metabolic labeling applications and provide the foundation for clearer insight into cellular RNA dynamics through the improvement of all the methods listed above.

DESIGN

We sought chemistry to enrich s^4U-RNA that satisfied several considerations. First, the chemistry should be efficient, leading to high yields of labeled s^4U residues. To maintain the advantages of reversible covalent chemistry, we focused on activated disulfide reagents, which allow reductive release after enrichment. This labeling chemistry should be rapid, minimizing time required for purification and decreasing RNA degradation during handling. Finally the chemistry needs to be specific for s^4U and should not react with RNA that lacks

thiol groups. These improvements would lead to a more robust protocol for s^4U-RNA isolation. Additionally, optimized chemistry could allow the extension of labeling to small RNAs including miRNAs. Smaller RNAs are expected to be particularly sensitive to the efficiency of s^4U labeling, as they tend to have fewer uridine residues and therefore have lower probability of successful labeling. To develop chemistry that meets the above criteria, we first used simple chemical systems to determine the reactivity of activated disulfides. We studied the specificity of labeling chemistry using synthetic RNA with and without s^4U. We used metabolic labeling experiments together with RNA-sequencing (RNA-Seq) to test the application of this chemistry in the context of complex RNA samples. Finally, we evaluated the use of this chemistry to study miRNA turnover, revealing fast- and slow-turnover miRNAs in proliferating cells without perturbing miRNA processing pathways.

RESULTS

Optimizing labeling chemistry using free nucleosides

To examine the reactivity of s^4U-RNA with HPDP-biotin, we first studied the labeling of the s^4U nucleoside using liquid chromatography coupled to mass spectrometry (LC-MS; Figure 1A, B). We found biotinylation of the s^4U nucleoside with HPDP-biotin to be inefficient when using buffer conditions that are commonly used in the retrieval of s^4U-RNA (Gregersen et al., 2014). This inefficiency stems from the forward and reverse disulfide exchange reactions (Figure 1A). Any disulfide formed with the electron-poor pyrimidine ring of s^4U results in a more activated product, therefore favoring the reverse rather than the forward labeling reaction. For this reason, it is not surprising that HPDP-biotin is an inefficient reagent for disulfide exchange with s^4U. Improving this chemistry would expand the utility of s^4U, improve the sensitivity of s^4U labeling, and reduce bias in s^4U-RNA enrichment.

Of the numerous activating chemistries used to make asymmetric disulfides (Jeschke, 2013; Kenyon and Bruice, 1976), thiosulfates and alkylthiosulfonates are particularly attractive (Figure 1C). We found that, in sharp contrast to the slow and inefficient reaction with HPDP-biotin, methylthiosulfonate-activated biotin (MTS-biotin) reacts efficiently with s^4U, leading to >95% conversion to the mixed disulfide within just five minutes (Figure 1D). We validated this difference in s^4U reactivity between MTS-reagents and 2-pyridylthio-activated disulfides using NMR (Figure 1E, Figure S1A–S1C). While only a minority of s^4U reacted using 2-pyridylthio chemistry (<20%), MTS chemistry led to >95% conversion of s^4U to the mixed disulfide.

Extending MTS labeling chemistry to s^4U-RNA

This MTS-chemistry could be used to specifically fluorescently label s^4U-RNA in the context of cell extracts (Figure S1D). Furthermore, we found that the use of MTS-biotin leads to superior biochemical enrichment of s^4U-RNA in comparison to HPDP-biotin (compare flow through to eluent in Figure 1F, G) or thiosulfate-biotin (TS-biotin, Figure S1E–G). Importantly, MTS- and HPDP-chemistries are specific for enrichment of s^4U, as no significant enrichment of RNA without s^4U occurred in either case (Figure 1F, G, Figure

S1H). We therefore conclude that MTS-chemistry provides a specific and highly efficient means of detecting and biochemically purifying s^4U-RNA.

We next tested the efficacy of MTS-biotin as a reagent to examine newly transcribed RNA in HEK293T cells (Figure 2A). We treated cells with s^4U-supplemented media and reacted the isolated RNA with either HPDP-biotin (as described previously by(Gregersen et al., 2014) or MTS-biotin. Biotinylated RNA was enriched and then analyzed by RNA-sequencing (RNA-Seq). To compare the RNA-Seq reads across experiments, we used a normalization approach developed by Sun *et al*. (2012) in which the same amount of RNA from *S. pombe* is added to each sample prior to constructing the library for RNA-Seq. Consistent with our prior analysis, compared to HPDP-biotin, the use of MTS-biotin led to significantly greater normalized coverage of the human transcriptome (Figure 2B, C). This enrichment was reproducible across biological replicates (Pearson's $r = 0.92$, Figure S2A–D) and was validated by qPCR (Figure S2E, F). To test the specificity of MTS chemistry, we examined MTS-biotin treated RNA from cells that had not been treated with s^4U, and found substantially fewer normalized reads than with either HPDP-biotin or MTS-biotin enriched s^4U-RNA (Figure 2B, C). The result from this control experiment validated the specificity of MTS-biotin for metabolically labeled s^4U-RNA.

Alleviating length bias using MTS-biotin

We next compared the distributions of enriched RNAs using MTS- and HPDP-biotin. Purification of s^4U-RNA using HPDP-biotin is reported to bias enrichment toward longer RNAs that tend to contain increasing numbers of uridines, hereafter referred to as length bias (Miller et al., 2011; Miller et al., 2009). This bias was confirmed in our study (Figure 2D). While this bias can be partially mitigated statistically (Miller et al., 2011; Miller et al., 2009), more fruitful biochemical enrichment is clearly preferable, especially when examining overlapping transcript models of different sizes (*e.g.*, spliced and unspliced, see Supplemental Discussion). To examine how MTS chemistry impacted the length bias in comparison with other activated disulfides, we used an *in vitro* transcribed RNA ladder with and without s^4U to test the relative yields of RNAs with different lengths. This analysis confirmed the presence of a length bias, and agrees well with modeling results (Figure S1G), demonstrating how MTS chemistry largely alleviates length bias in RNA turnover experiments. Indeed, analysis of our RNA-Seq data reveals that MTS-biotin is less prone to length bias compared to HPDP-biotin (Figure 2D). For example, long transcripts like MALAT1 (8.7 kb) are isolated by HPDP-biotin and MTS-biotin with approximately equal efficiency, whereas shorter transcripts like SCYL1 and LTBP3 (2.3 kb and 3.4 kb, respectively, when fully spliced) are found at much greater levels in the MTS-biotin pulldown (Figure 2E).

Studying miRNA turnover using MTS-chemistry

Given the substantial increase in s^4U-RNA yields we observed when using MTS chemistry, we hypothesized that this chemistry could extend s^4U metabolic labeling to the study of miRNAs. The dynamics of miRNA biogenesis and degradation have gained interest because disruption of miRNA homeostasis is implicated in many diseases, particularly for miRNAs that regulate progression through the cell cycle (Chang and Mendell, 2007). Generally,

miRNA turnover has been investigated by blocking transcription or by inhibiting miRNA processing, followed by analysis of miRNA stability (Bail et al., 2010; Gantier et al., 2011; Guo et al., 2015). These approaches have demonstrated that while many miRNAs remain stable for tens of hours, there are also some miRNAs that turn over much more quickly (*e.g.*, miR-222). Extending these studies using metabolic labeling would allow the analysis of native miRNA levels in a proliferating system (unlike those studies using transcriptional block) without perturbing miRNA biogenesis or global miRNA levels (unlike studies where miRNA processing is blocked).

To investigate rates of global miRNA turnover, we treated HEK293T cells with s^4U for a range of times (Figure 3A) and enriched s^4U-miRNAs using MTS chemistry, followed by deep sequencing. To test whether s^4U perturbs miRNA steady-state levels, we examined miRNA levels in cells with and without s^4U treatment for 22 days, and we found high correlations in miRNA levels (Pearson's $r = 0.99$, Figure S3A), demonstrating that s^4U incorporation has minimal impact on miRNA levels. Our findings are consistent with previous accounts that s^4U causes minimal perturbation of longer transcripts (Gregersen et al., 2014; Hafner et al., 2010), and our own data with longer RNAs (Figure S3B). Consistent with our previous results and modeling, a positive control miRNA (a s^4U-miRNA spike-in added to cellular small-RNAs) was enriched when using MTS-biotin, but was not significantly enriched with HPDP-biotin (Figure S3D). We next evaluated the s^4U-miRNAs at different times after initiating s^4U treatment. We found miRNAs levels were reproducibly enriched from replicate samples (Figure 3C, S3E). Furthermore, miRNA levels in neighboring time points were most similar to each other, and those enriched at later time points (1 day, 3 day and 6 days) approached the levels observed at steady state (22 days). As expected, the steady-state miRNA levels most closely resembled the input miRNAs levels (Figure 3C).

To determine which miRNAs turned over most quickly, we analyzed the relative distribution of enriched miRNAs at early time points (20 min) versus steady state (6 days or greater; Figure 3D). We identified many RNAs whose relative enrichment was significantly different from steady state at early time points, and found these miRNAs displayed a consistent trend across time (Figure 3E). We expect fast-turnover miRNAs to be over-represented relative to the population in early time points, and slow-turnover miRNAs to be under-represented (Figure 3B). To evaluate this expectation, we took advantage of established properties of miRNA processing (reviewed in(Rüegger and Großhans, 2012; Winter et al., 2009). During miRNA biogenesis, one of the two strands from the duplex precursor generally degrades rapidly (referred to here as the miR-star) while the other strand is incorporated into the RNA-induced silencing complex (RISC) and exhibits higher stability. Therefore, we hypothesized that the miR-star sequences would be over-represented at early time points, and this hypothesis was verified: of the 52 significantly enriched and depleted miRNAs (FDR < $5x10^{-5}$), about one third of the fast-turnover miRNAs were miR-star sequences (11/30), while none of the stable miRNAs (0/22) were annotated as miR-star sequences. The fast-turnover miRNAs we identified include miRNAs that agree with previous results using transcriptional blockade (*e.g.*, miR-222; Guo et al, 2015). Other miRNAs were found to be slow turnover (*e.g.*, miR-7), and many of these are also in agreement with past studies (Bail

et al., 2010; Guo et al., 2015). In general, our results using metabolic labeling of miRNAs agree well with results from analysis of degradation after blocking miRNA production (Bail et al., 2010; Guo et al., 2015). There are exceptions, however, such as miR-98-5p and miR-191-5p, which were identified as fast-turnover miRNAs in our analysis (Figure 3D, E, and Figure S3F for qPCR validation; for a full list of fast-turnover non-star miRNAs, see Table S2), yet upon transcriptional blockade these miRNAs are stable (Bail et al., 2010; Guo et al., 2015). While these results may be due to tissue or cell line differences, it is more likely the faster turnover we observed for miR-98-5p and miR-191-5p is due to the cell cycle regulation of these miRNAs (Polioudakis et al., 2015; Ting et al., 2013). Turnover in response to progression through the cell cycle is masked when using transcriptional inhibition, but this turnover is evident using a metabolic labeling approach to study miRNA dynamics in dividing cells, underscoring one of the advantages of this improved chemistry.

DISCUSSION

Together, our results demonstrate that MTS-biotin is a specific reagent that can be used to efficiently label and enrich s^4U-RNA with higher yields and less bias than the commonly used HPDP-biotin. The dramatic improvement over existing s^4U biotinylation protocols renders MTS chemistry useful for studying dynamics of free nucleosides (Figure 1B, D, E), synthetic RNAs (Figure 1F, G), *E. coli* extracts (Figure S1), and s^4U-RNA in metabolic labeling experiments (Figure 2). In RNA-turnover experiments, for example, the superior MTS chemistry alleviates transcript length bias, decreases the amount of starting material required, and may allow for the use of lower doses of s^4U to avoid potential toxicities that some have observed (Burger et al., 2013), but not others (Gregersen et al., 2014; Hafner et al., 2010), when metabolically labeling cells. We demonstrate the utility of this MTS chemistry using miRNA RATE-seq, which allowed us to identify fast- and slow-turnover miRNAs in proliferating cells with flux through the miRNA pathway (Figure 3). This advance provides the foundation for more detailed kinetic analyses of miRNA processing and turnover. More generally, applying the chemistry described herein should provide a superior means to gain insights into RNA dynamics in diverse biological systems.

LIMITATIONS

This manuscript describes improved capture of s^4U-RNA, but the enrichment will only be successful when the RNA contains sufficient levels of s^4U. In metabolic labeling experiments, incorporation of s^4U into RNA can be controlled by the concentration of s^4U during cell treatment and the time of s^4U exposure. Insufficient s^4U incorporation leads to low yields and will also favor enrichment of longer transcripts that have more uridine residues (and therefore a greater probability of s^4U incorporation). For technical considerations while preforming s^4U-RNA enrichment see Experimental Procedures and the Detailed Protocol included in the Supplemental Material.

EXPERIMENTAL PROCEDURES

Cell lines and s^{4}U metabolic labeling

HEK293T cells were cultured in high glucose DMEM media supplemented with 10% (v/v) fetal bovine serum, and 1% (v/v) 2 mM L-glutamine. For labeling of long RNAs, cultured cells at 80% confluence were treated with 700 μM s^{4}U for 60 min, washed with PBS, trypsinized, and harvested. Cells were resuspended in TRIzol reagent, flash frozen, and stored overnight at −80°C. Cell lysates were chloroform extracted once and total RNA was purified by the RNeasy mini kit (Qiagen). For miRNA labeling, cultured cells were grown for 6 days and split 1:8 on day 3. Cells were grown in the presence of 100 μM s^{4}U for 22 days, 6 days, 3 days, 1 day, 9 hr, 3 hr, 1 hr, 20 min, or in the absence of s^{4}U. On day 6, all cells were harvested using trypsin and resuspended in TRIzol reagent with exogenous s^{4}U-containing miRNAs (Dharmacon) and one exogenous non-s^{4}U miRNA (IDT). Samples were flash frozen, and stored overnight at −80°C. Cell lysates were chloroform extracted once and total RNA purified by the miRvana miRNA isolation kit (Life Technologies).

Purification of s^{4}U-labeled RNA

Biotinylation and s^{4}U-RNA enrichment with HPDP-biotin were carried out based on protocols adapted from Gregersen *et al*. and optimized for MTS-biotin. Reactions were carried out in a total volume of 250 μL, containing 70 μg total RNA, 10 mM HEPES [pH 7.5], 1 mM EDTA, and 5 μg MTSEA biotin-XX (Biotium) or 50 μg HPDP-biotin (Pierce) freshly dissolved in DMF (final concentration of DMF = 20%). Reactions were incubated at room temperature for 2 hr (HPDP) or 30 min (MTS) in the dark. Following biotinylation, excess biotin reagents were removed by addition of 1 volume phenol:chloroform (Sigma), followed by vigorous mixing for 15 seconds, 2 min incubation at RT, and centrifugation in a Phase-Lock-Gel tube (5Prime) at 12,000 x g for 5 min. Supernatant was removed and RNA was precipitated with a 1:10 volume (20 uL) of 5 M NaCl and an equal volume of isopropanol (200 uL) and centrifuged at 20,000 x g for 20 min. The pellet was washed with an equal volume of 75% ethanol. Purified RNA was dissolved in 50 μL RNase-free water and denatured at 65°C for 10 min, followed by rapid cooling on ice for 5 min. Biotinylated RNA was separated from non-labeled RNA using μMacs Streptavidin Microbeads (Miltenyi). Beads (200 μL) were added to each sample and incubated for 15 min at room temperature. In the meantime, μColumns were placed in the magnetic field of the μMacs separator and were equilibrated with nucleic acid wash buffer supplied with the beads (Miltenyi). Reactions were applied to the μColumns and flow-through was collected as the pre-existing RNA fraction. μColumns were washed twice with high salt wash buffer (500 μL each, 100 mM Tris-HCl [pH 7.4], 10 mM EDTA, 1 M NaCl, and 0.1% Tween-20). s^{4}U-RNA was eluted from μColumns with 100 μL freshly prepared 100 mM DTT followed by a second elution with an additional 100 μL 5 min later. RNA was recovered from the flow-through and eluent samples using the MinElute Spin columns (Qiagen) according to the instructions of the manufacturer. *S. pombe* total RNA (11 ng, a generous gift from Julien Berro) was added to each sample for downstream normalization.

s^{4}U-Seq library preparation and sequencing

All sequencing libraries were constructed using standard protocols by the Yale Center for Genomic Analysis (YCGA) and run on Illumina HiSeq 2500 instruments. For long RNA-Seq, strand-specific polyA selected RNA-Seq 5 μg of input and RNA collected from flow-through and eluted fractions. Samples were multiplexed using Illumina bar codes and sequenced using paired-end 2 x 75-nt cycles. For small RNA-Seq, 10% input and RNA collected from eluted fractions were used for small RNA library preparation and sequenced with single-end 75-nt cycles.

Mapping and quantification of s^{4}U-Seq libraries

For long RNA-Seq, sequencing reads were aligned using Tophat2 (version 2.0.12; Bowtie2 version 2.2.3), to a joint index of the *H. sapiens* and *S. pombe* genomes (hg19 and PomBase v22) and transcriptomes (GENCODE v19 and Ensembl Fungi v22; Harrow et al., 2012 and Kersey et al., 2013, respectively). Alignments and analysis were performed on the Yale High Performance Computing clusters. Following this, we used Cufflinks (version 2.2.1; Trapnell et al., 2010) to quantify annotated *H. sapiens* and *S. pombe* transcripts, using only reads that were uniquely mapped (MAPQ > 20) and that aligned with up to two mismatches to the reference.

s^{4}U-Seq normalization

To compare transcript levels between samples, we normalized expression values to *S. pombe* spike-ins as follows:

$$FPKM_{norm} = FPKM_{raw} S_{norm}$$

Where $FPKM_{norm}$ is the normalized FPKM of a human transcript or gene, $FPKM_{raw}$ is the original FPKM calculated for the sample of interest, and S_{norm} is the slope of the linear regression line of raw *S. pombe* gene FPKMs with the normalizing sample on the y-axis and the sample of interest on the *x*-axis (Figure S2B, Table S1). To normalize genomic coverage tracks, we used a similar scheme:

$$Coverage_{norm} = Coverage_{raw} S_{norm} \frac{R_{sample}}{R_{norm}}$$

Where $Coverage_{norm}$ and $Coverage_{raw}$ are the normalized and raw read coverages at a given genomic position, and R_{sample} and R_{norm} are the numbers of unique reads in the sample of interest and the normalizing sample, respectively. The $\frac{R_{sample}}{R_{norm}}$ adjustment factor reflects that we are comparing raw reads, instead of FPKMs. We generated stranded genomic coverage tracks using IGVTools (version 2.3.32; Thorvaldsdóttir et al., 2013). For all analyses, we normalized to the *S. pombe* spike in the HPDP-biotin sample. We also accounted for the ten-fold biochemical dilution of the input samples prior to library preparation by multiplying normalized values for these samples by ten.

Assessment of length bias in eluted s^{4}U-Seq RNA

Because incorporation and biotinylation of s^{4}U are not perfectly efficient, especially when using HPDP-biotin, it is expected that transcripts with more uridines will be purified at rates greater than or equal to those of shorter transcripts. To assess length bias for each reagent, we binned transcript isoforms by numbers of uridines present, and compared the fractions of total input RNA that were purified between bins using the Wilcoxon rank-sum test. To avoid noise from misassignment of reads between isoforms of individual genes, we included only the dominant isoforms of genes (>90% of total expression) in all samples included in the analysis. We only included transcripts greater than 200-nt, since shorter transcripts were biochemically depleted in the library preparation, and removed transcripts with expression levels in the bottom quartile of the input sample.

qPCR assays

For qPCR analysis of long RNA, input or enriched RNA was converted into cDNA with VILO reverse-transcription kit (Life Technologies). qPCR was carried out on the CFX96 real-time system (BioRad) with the iTaq Universal SYBR Green Mix. Results from all primers used (listed in Table S3) were corrected for amplification efficiency. For miRNA analysis, qPCR was performed using TaqMan miRNA assays (Life Technologies) according to the instructions of the manufacturer for the following targets: hsa-miR-7, UGGAAGACUAGUGAUUUUGUUG; hsa-miR-20a, UAAAGUGCUUAUAGUGCAGGUAG; hsa-miR-98, UGAGGUAGUAAGUUGUA UUGUU; hsa-miR-99b, CACCCGUAGAACCGACCUUGCG; hsa-miR-191, CAACGGAAUC CCAAAAGCAGCUG; hsa-miR-222, AGCUACAUCUGGCUACUGGGUCUC; EED004r, CC AUUUGUAUGUUCGGCUAACU; and EED095r; CCAUUUCGCUCGGGUGCUAACU.

miRNA RATE-seq s^{4}U RNA enrichment

Biotinylation and s^{4}U-RNA enrichment were carried out as described above (Purification of s^{4}U-labeled RNA) with the following modifications. Excess biotinylation reagent was removed using a nucleotide cleanup kit (Qiagen). Following enrichment, RNA was concentrated by ethanol precipitation and resuspended in 14 μL RNase-free water. After enrichment, samples were supplemented with four synthetic miRNA standards (Dharmacon; Table S3).

miRNA RATE-seq bioinformatic analysis

To analyze our smRNA RATE-Seq data, we used a hierarchical mapping pipeline combining the sRNAbench (Rueda et al., 2014), Bowtie (Langmead et al., 2009), and Bowtie2 tools (Langmead and Salzberg, 2011). Before mapping the reads, we removed sequencing adapters, using fastx-clipper (http://hannonlab.cshl.edu/fastx_toolkit/). We then proceeded to use Bowtie2 to map reads first to synthetic spikes, and then to the UniVec laboratory contaminant database (http://www.ncbi.nlm.nih.gov/tools/vecscreen/univec/) and ribosomal RNAs from the GENCODE v19 annotation (Harrow et al., 2012). These two categories of sequences that are not expected to produce reads in our miRNA libraries, except by contamination or RNA degradation. The remaining unmapped reads were then

mapped using sRNAbench, first to the miRBase miRNA 21 annotation (Kozomara and Griffiths-Jones, 2013), and then to the entire human genome (hg19). Input reads under 19-nt or with greater than one mismatch were removed from all analyses of miRNA and spike quantifications.

To perform differential expression analysis between smRNA RATE-Seq time points, we used the edgeR package (version 3.2.4; Robinson et al., 2010; Robinson and Smyth, 2007). Specifically, we compared three early time points (both 20 min replicates and a deeply sequenced 1 hr time point) to three late time points (two 6 day replicates and a 22 day sample). miRNA read counts and dispersions were fit to a negative binomial distribution, and differential expression was evaluated using the negative binomial exact test. To correct for multiple hypothesis testing, we used the Bonferroni correction, and set a family-wise error rate of 0.005 to select differentially expressed miRNAs between early time points and the steady state.

Mass spectrometry of s^4U disulfide exchange

Reactions (50 μL) contained s^4U (50 μM), buffer (20 mM HEPES [pH 7.5], 1 mM EDTA), and MTS- or HPDP-biotin (5 mM) dissolved in DMF (final concentration of DMF = 5%). Aliquots were taken at designated time points and analyzed on an Agilent 6650A Q-TOF using a reverse phase column (Thermo Scientific Hypersil GOLD 3 μm, 160 x 2.1 mm) detected by electrospray ionization (positive ion mode). Chromatography conditions were established based on Sun *et al*. 2014. Briefly, analysis was initiated with an isocratic gradient of 100% buffer A at 0.4 mL/min for 6 min followed by a linear gradient of 0–50% buffer B over 6 min, 50–75% buffer B over 2 min, then an isocratic elution at 75% buffer B (buffer A: H_2O in 0.1% (vol/vol) formic acid; buffer B: acetonitrile in 0.1% (vol/vol) formic acid).

NMR of s^4U disulfide exchange

Reactions (600 μL) were preformed in D_2O containing 10 mM HEPES, s^4U (1 mg, 6.4 mM) and five equivalents of MeMTS or PDPH dissolved in DMF-δ_7 (60 μL, 10% total volume). These reactions were incubated in the dark 2 hr for PDPH and 30 min for MeMTS. Reactions were analyzed on an Agilent DD2 400 MHz NMR with 16 scans.

Enrichment of singly thiolated RNA

Two fluorescently labeled RNAs were synthesized for s^4U enrichment: non-s^4U 39-nt RNA (DY647 - GGAACCGCCCGGAUAGUGUCCUUGGGAAACCAAGUCCGGGCACCA) and one s^4U 39-nt RNA (DY547 - GGAACCGCCCGGA(s^4U)AGUGUCCUUGGGAAACCAAGUCCGGGCACCA) (Dharmacon). Biotinylation reactions (50 μL total) contained RNA (1 μM), 10 mM HEPES [pH 7.5], 1 mM EDTA, and 25 μM MTS- or HPDP-biotin (dissolved in DMF at 250 μM). Reactions were incubated at room temperature in the dark for 30 min or 2 hr, respectively. Following biotinylation, excess biotinylation reagenets were removed with two consecutive chloroform washes, followed by purification with a nucleotide cleanup kit (Qiagen) according to the manufacturer's instructions. Biotinylated RNA was separated from non-labeled RNA using Dynabeads MyOne Streptavidin C1 beads (Invitrogen). Biotinylated

RNA was incubated with 50 μL Dynabeads with rotation for 1 hr at room temperature in the dark. Beads were magnetically fixed and washed twice with Dynabeads high salt wash buffer. s^4U-RNA was eluted with 100 μL of elution buffer (10 mM Tris [pH 7.4] and 100 mM DTT). Fractions were concentrated by ethanol precipitation, separated on a 12% urea-PAGE gel, and visualized by Typhoon fluorescence imager (GE).

Enrichment of an *in vitro* transcribed RNA ladder

An RNA ladder of 100–1000 nt was transcribed *in vitro* using the RNA Century Plus Marker Template and Maxiscript T7 transcription kit (Invitrogen) using Cy5-CTP at a ratio of 1:1 Cy5-CTP:CTP for downstream visualization, with the option of adding s^4UTP (TriLink Biotechnologies) at a ratio of s^4UTP:UTP to the reaction. After the reaction, excess nucleotides were removed by an Illustra Microspin G-25 column (GE Healthcare Life Sciences) according to the manufacturer's instructions. RNA ladders were reacted with HPDP-, MTS- or thiolsulfonate-biotin (Biotium), following the protocol described above. Enriched samples were separated on a 5% urea-PAGE gel, stained with GelGreen and visualized by Typhoon fluorescence imager (GE).

Enrichment of thiolated tRNA from *E. coli*

E. coli WT and Δ*thiI* cultures were grown to mid-log phase in LB media. Strains were a generous gift from Eugene Mueller (Mueller et al., 1998). Cells were pelleted at 3,250 x g for 10 min at 4°C. Total RNA was purified by the mirVana miRNA isolation kit (Life Technologies). RNA pulldowns were performed as above (Purification of s^4U-labeled RNA) and fractions separated on a 5% urea-PAGE gel, followed by visualization with GelGreen stain.

Supplementary Material

Refer to Web version on PubMed Central for supplementary material.

Acknowledgments

We thank J. Steitz, P. Sung, S. Strobel, D. Canzio, and members of the Simon and Gerstein labs for helpful discussions and comments on the manuscript, and T. Wu, H. Jamali, and M. Xie for assistance with mass spectrometry, NMR, and sequencing validation, respectively. This work was supported by the NIH grant DP2 1DP2HD083992 (M.D.S.), the Searle Scholars Program (M.D.S.), NSF Graduate Research Fellowship (E.E.D.), and the Yale Science Scholars (C.D.S.).

References

Bail S, Swerdel M, Liu H, Jiao X, Goff LA, Hart RP, Kiledjian M. Differential regulation of microRNA stability. RNA. 2010; 16:1032–1039. [PubMed: 20348442]

Burger K, Mühl B, Kellner M, Rohrmoser M, Gruber-Eber A, Windhager L, Friedel CC, Dölken L, Eick D. 4-thiouridine inhibits rRNA synthesis and causes a nucleolar stress response. RNA Biol. 2013; 10:1623–1630. [PubMed: 24025460]

Chang TC, Mendell JT. microRNAs in vertebrate physiology and human disease. Annual Reviews of Genomics and Human Genetics. 2007; 8:215–239.

Cleary M, Meiering C, Jan E, Guymon R, Boothroyd J. Biosynthetic labeling of RNA with uracil phosphoribosyltransferase allows cell-specific microarray analysis of mRNA synthesis and decay. Nat Biotechnol. 2005; 23:232–237. [PubMed: 15685165]

Dölken L, Ruzsics Z, Rädle B, Friedel C, Zimmer R, Mages J, Hoffmann R, Dickinson P, Forster T, Ghazal P, et al. High-resolution gene expression profiling for simultaneous kinetic parameter analysis of RNA synthesis and decay. RNA. 2008; 14:1959–1972. [PubMed: 18658122]

Fuchs G, Voichek Y, Benjamin S, Gilad S, Amit I, Oren M. 4sUDRB-seq: measuring genomewide transcriptional elongation rates and initiation frequencies within cells. Genome Biol. 2014; 15:R69. [PubMed: 24887486]

Gantier MP, McCoy CE, Rusinova I, Saulep D, Xu D, Irving AT, Behlke MA, Hertzog PJ, Mackay F, Williams BRG. Analysis of microRNA turnover in mammalian cells following Dicer1 ablation. Nucleic Acids Res. 2011; 39:5692–5703. [PubMed: 21447562]

Gregersen L, Schueler M, Munschauer M, Mastrobuoni G, Chen W, Kempa S, Dieterich C, Landthaler M. MOV10 Is a 5′ to 3′ RNA helicase contributing to UPF1 mRNA target degradation by translocation along 3′ UTRs. Mol Cell. 2014; 54:573–585. [PubMed: 24726324]

Guo Y, Liu J, Elfenbein SJ, Ma Y, Zhong M, Qiu C, Ding Y, Lu J. Characterization of the mammalian miRNA turnover landscape. Nucleic Acids Res. 2015; 43:2326–2341. [PubMed: 25653157]

Hafner M, Landthaler M, Burger L, Khorshid M, Hausser J, Berninger P, Rothballer A, Ascano M Jr, Jungkamp AC, Munschauer M, et al. Transcriptome-wide identification of RNA-binding protein and microRNA target sites by PAR-CLIP. Cell. 2010; 141:129–141. [PubMed: 20371350]

Harrow J, Frankish A, Gonzalez JM, Tapanari E, Diekhans M, Kokocinski F, Aken BL, Barrell D, Zadissa A, Searle S, et al. GENCODE: The reference human genome annotation for The ENCODE Project. Genome Res. 2012; 22:1760–1774. [PubMed: 22955987]

Jao CY, Salic A. Exploring RNA transcription and turnover in vivo by using click chemistry. P Natl Acad Sci USA. 2008; 105:15779–15784.

Jeschke G. Conformational dynamics and distribution of nitroxide spin labels. Prog Nucl Mag Res Sp. 2013; 72:42–60.

Kenyon GL, Bruice TW. Novel sulfhydryl reagents. Method Enzymol. 1976; 47:407–430.

Kersey PJ, Allen JE, Christensen M, Davis P, Falin LJ, Grabmueller C, Hughes DS, Humphrey J, Kerhornou A, Khobova J, et al. Ensembl Genomes 2013: scaling up access to genome-wide data. Nucleic Acids Res. 2013; 42:52.

Kozomara A, Griffiths-Jones S. miRBase: annotating high confidence microRNAs using deep sequencing data. Nucleic Acids Res. 2013; 42:D68–73. [PubMed: 24275495]

Langmead B, Salzberg SL. Fast gapped-read alignment with Bowtie 2. Nat Methods. 2011; 9:357–359. [PubMed: 22388286]

Langmead B, Trapnell C, Pop M, Salzberg SL. Ultrafast and memory-efficient alignment of short DNA sequences to the human genome. Genome Biol. 2009; 10:R25. [PubMed: 19261174]

Melvin WT, Milne HB, Slater AA, Allen HJ, Keir HM. Incorporation of 6-thioguanosine and 4-thiouridine into RNA. Application to isolation of newly synthesised RNA by affinity chromatography. Eur J Biochem / FEBS. 1978; 92:373–379.

Miller C, Schwalb B, Maier K, Schulz D, Dümcke S, Zacher B, Mayer A, Sydow J, Marcinowski L, Dölken L, et al. Dynamic transcriptome analysis measures rates of mRNA synthesis and decay in yeast. Mol Syst Biol. 2011; 4:458. [PubMed: 21206491]

Miller MR, Robinson KJ, Cleary MD, Doe CQ. TU-tagging: cell type-specific RNA isolation from intact complex tissues. Nature methods. 2009; 6:439–441. [PubMed: 19430475]

Mueller E, Buck C, Palenchar P, Barnhart L, Paulson J. Identification of a gene involved in the generation of 4-thiouridine in tRNA. Nucleic Acids Res. 1998; 26:2606–2610. [PubMed: 9592144]

Neymotin B, Athanasiadou R, Gresham D. Determination of in vivo RNA kinetics using RATE-seq. RNA. 2014; 20:1645–1652. [PubMed: 25161313]

Polioudakis D, Abell NS, Iyer VR. MiR-191 regulates primary human fibroblast proliferation and directly targets multiple oncogenes. PLoS ONE. 2015; 10:e0126535. [PubMed: 25992613]

Rabani M, Levin J, Fan L, Adiconis X, Raychowdhury R, Garber M, Gnirke A, Nusbaum C, Hacohen N, Friedman N, et al. Metabolic labeling of RNA uncovers principles of RNA production and degradation dynamics in mammalian cells. Nat Biotechnol. 2011; 29:436–442. [PubMed: 21516085]

Robinson MD, McCarthy DJ, Smyth GK. edgeR: a Bioconductor package for differential expression analysis of digital gene expression data. Bioinformatics. 2010; 26:139–140. [PubMed: 19910308]

Robinson MD, Smyth GK. Moderated statistical tests for assessing differences in tag abundance. Bioinformatics. 2007; 23:2881–2887. [PubMed: 17881408]

Rueda A, Barturen G, Lebrón R, Gómez-Martín C, Alganza Á, Oliver JL, Hackenberg M. sRNAbench: profiling of small RNAs and its sequence variants in single or multi-species high-throughput experiments. Methods Next Gen Seq. 2014; 43:W467–W473.

Rüegger S, Großhans H. MicroRNA turover: when, how, and why. Trends Biochem Sci. 2012; 37:436–446. [PubMed: 22921610]

Sun M, Schwalb B, Schulz D, Pirkl N, Etzold S, Larivière L, Maier K, Seizl M, Tresch A, Cramer P. Comparative dynamic transcriptome analysis (cDTA) reveals mutual feedback between mRNA synthesis and degradation. Genome Res. 2012; 22:1350–1359. [PubMed: 22466169]

Tani H, Akimitsu N. Genome-wide technology for determining RNA stability in mammalian cells: historical perspective and recent advantages based on modified nucleotide labeling. RNA Biol. 2012; 9:1233–1238. [PubMed: 23034600]

Tani H, Mizutani R, Salam KA, Tano K, Ijiri K, Wakamatsu A, Isogai T, Suzuki Y, Akimitsu N. Genome-wide determination of RNA stability reveals hundreds of short-lived noncoding transcripts in mammals. Genome Res. 2012; 22:947–956. [PubMed: 22369889]

Thorvaldsdóttir H, Robinson JT, Mesirov JP. Integrative Genomics Viewer (IGV): high-performance genomics data visualization and exploration. Brief Bioinform. 2013; 14:178–192. [PubMed: 22517427]

Ting H-J, Messing J, Sayeda Y-K, Lee Y-F. Identification of microRNA-98 as a Therapeutic Target Inhibiting Prostate Cancer Growth and a Biomarker Induced by Vitamin D. J Biol Chem. 2013; 288:1–9. [PubMed: 23188821]

Trapnell C, Williams BA, Pertea G, Mortazavi A, Kwan G, van Baren MJ, Salzberg SL, Wold BJ, Pachter L. Transcript assembly and quantification by RNA-Seq reveals unannotated transcripts and isoform switching during cell differentiation. Nat Biotechnol. 2010; 28:511–515. [PubMed: 20436464]

Winter J, Jung S, Keller S, Gregory RI, Diederichs S. Many roads to maturity: microRNA biogenesis pathways and their regulation. Nat Cell Biol. 2009; 11:228–234. [PubMed: 19255566]

Highlights

- Current methods to track s^4U-RNA are inefficient, giving low yields and high bias.
- MTS-chemistry efficiently labels s^4U-RNA, which improves methods that rely on s^4U.
- Increased sensitivity provides greater insight into RNA dynamics and miRNA turnover.

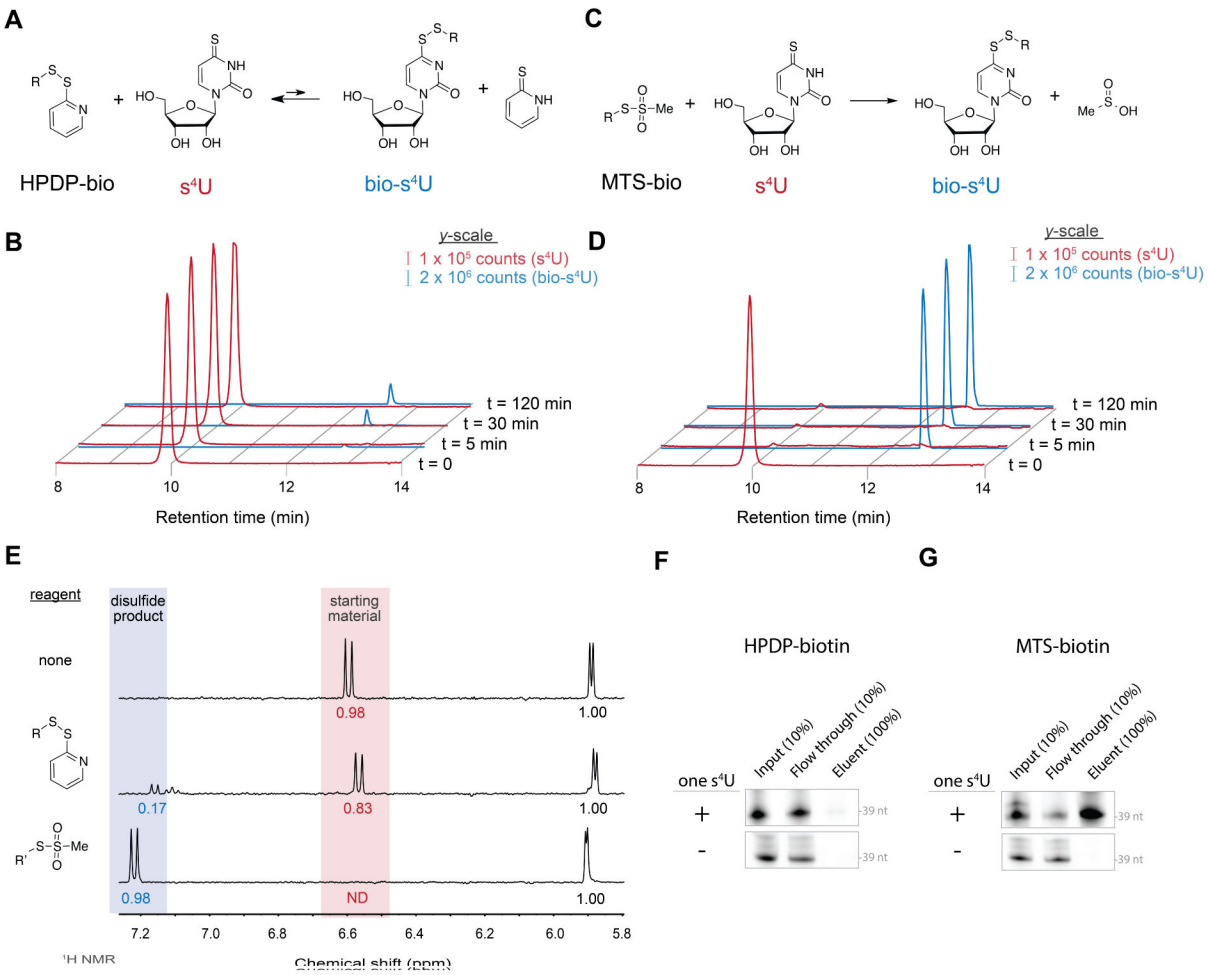

Figure 1. Efficient formation of disulfides with s^{4}U via MTS chemistry

(A) s^{4}U disulfide exchange with HPDP-biotin. (B) LC-MS extracted ion chromatograms of s^{4}U (red) and biotin-s^{4}U (blue) for HPDP-biotin at the indicated reaction times. (C) s^{4}U disulfide exchange with MTS-biotin. (D) LC-MS chromatograms as in (B). (E) Downfield ^{1}H NMR spectra of (top) s^{4}U alone, (center) s^{4}U reacted with 3-[2-Pyridyldithio]propionyl hydrazide (PDPH), an HPDP-like disulfide, and (bottom) methyl-MTS. Peaks for the starting material (red shading) and products (blue shading) were integrated and normalized to sum of the anomeric protons of s^{4}U and its products (5.9 ppm). For full spectra, see Figure S1A–C. (F, G) Enrichment of a singly-thiolated 39-nt RNA by (F) HPDP-biotin or (G) MTS-biotin. Fluorescently labeled 39-nt RNAs with or without a single s^{4}U were biotinylated with the indicated reagent and enriched on streptavidin beads, followed by urea-PAGE and fluorescence imaging. See also Figure S1.

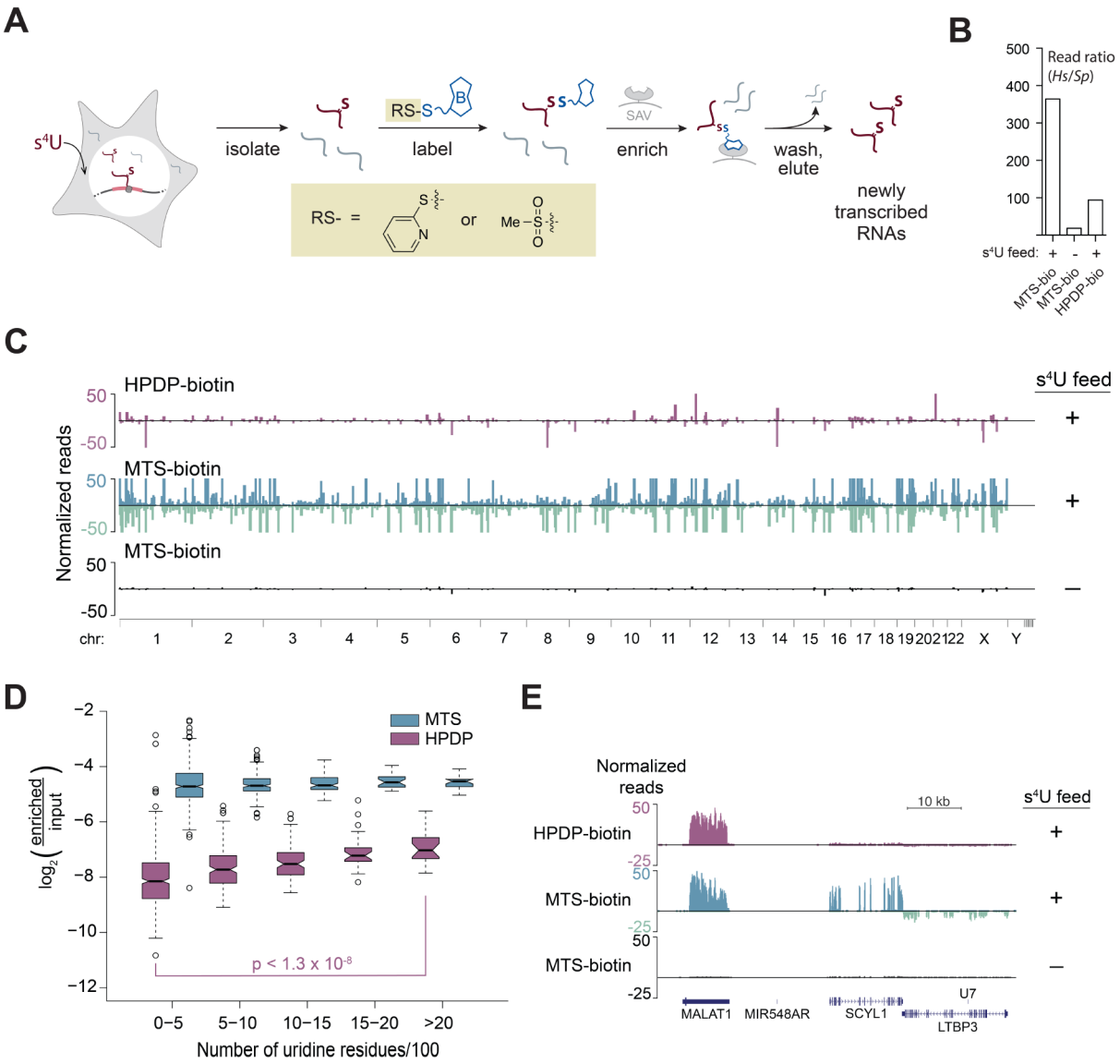

Figure 2. MTS-biotin affords higher specific yields and lower length bias of s^{4}U-RNA

(A) Schematic of s^{4}U metabolic labeling. 293T cells were treated with s^{4}U (700 μM) for one hour, followed by total RNA extraction, biotinylation with either HPDP- or MTS-biotin, and enrichment on streptavidin-coated magnetic resin. (B) Total reads for each RNA-Seq sample that mapped to the *H. sapiens* genome, divided by total number of reads that mapped to the *S. pombe* genome. (C) Whole genome alignments of eluted samples from HPDP- or MTS-biotin enrichments. *y*-axis indicates number of reads normalized by *S. pombe* spike-ins (see Materials and Methods). Forward and reverse strand reads are represented as positive and negative values on the *y*-axis respectively. To compare coverage between samples on the same *y*-axis scale, in some cases, read coverage exceeds the *y*-axis upper limit in MTS-biotin (127 cases) and HPDP-biotin (4 cases). Chromosomes are indicated below the mapped reads. (D) Box plot of transcripts recovered by MTS-biotin and HPDP-biotin binned by transcript length. Blue = MTS-biotin, purple = HPDP-biotin. (E) Examples of genes

enriched by HPDP- and MTS-biotin, along with a no s^4U-feed control. MALAT1 (8.7 kb), SCYL1 (2.3 kb cDNA) and LTBP3 (3.4 kb cDNA) gene architectures displayed below. See also Figure S2, Table S1.

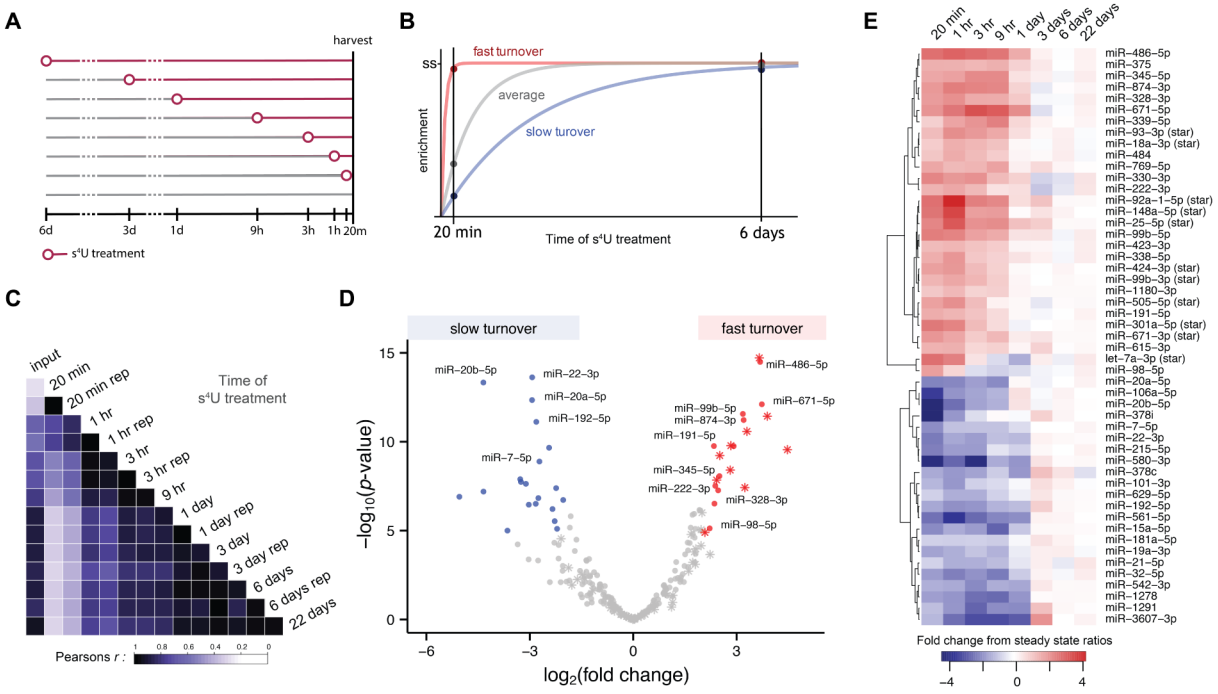

Figure 3. MTS chemistry reveals fast- and slow-turnover miRNAs in miRNA RATE-seq experiments

(A) Schematic of s^4U treatments used in miRNA RATE-seq. (B) Cartoon of anticipated behavior of fast-turnover and slow-turnover miRNAs in comparison to average. Fast-turnover miRNAs are expected to be over-represented in the early time points whereas slow-turnover miRNAs are depleted, relative to steady state (ss). (C) Heatmap depicting correlation coefficients (Pearson's *r*) between miRNA levels at different times after s^4U treatment. Replicate samples are indicated by (rep). (D) Volcano plot depicting results from a comparative analysis of miRNAs that are significantly enriched or depleted in early time points (20 min, 1 hr) relative to steady state levels (6 and 22 days). Fast-turnover miRNAs (fold difference early time points from steady state > 4; *p*-value < $2x10^{-5}$; Bonferroni family-wise error rate < 0.005) are colored red; slow-turnover miRNAs (fold difference early time points from steady state < 0.25; *p*-value < $2x10^{-5}$; Bonferroni family-wise error rate < 0.005) are shown in blue. Stars indicate miRNAs defined as miRNA-stars (see Experimental Procedures); the others are indicated with circles. (E) Heatmap indicating normalized miRNA enrichment relative to steady state level at each time point in RATE-seq for the fast- and slow-turnover miRNAs in (C). For clarity of presentation, the most significant fast-turnover miRNA in this analysis (miR-4521, $\log_2$(fold-change) = 10.8; *p*-value = $2.9x10^{-40}$) has been omitted from (C) and (D) due to values exceeding the indicated scales. See also Figure S5 and Table S2.